A phase-field model of dynamic fracture
Seminar Paper

Karsten Paul (333092)[a,*]

[a]*Computational Engineering Science (M.Sc.), RWTH Aachen University*
Supervisor: Christopher Zimmermann, M.Sc., AICES RWTH Aachen University

---

Abstract

Next to sharp interface models for the description and prediction of crack growth, diffuse interface models represent a powerful method so as to model cracks and their propagation. This work focuses on a phase-field description of dynamic fracture. Considering brittle fracture, the variational formulation of the problem is presented and the phase-field theory is introduced. The resulting coupled systems of partial differential equations are given. A fourth-order model is exposed by ~~manipulating~~ the crack density functional of the second-order model. In order to numerically approximate their solution, the semidiscrete Galerkin forms of the governing equations are derived. Since the fourth-order model require a higher ~~regularity~~ of the phase-field's solution, a ~~Finite Element Analysis~~ within an ~~Isogeometric Analysis~~ framework is outlined. A time integration scheme for the description of dynamic fracture ~~is sketched~~. ~~Finally,~~ the major differences between sharp and diffuse interface models are examined ~~and consequently, advantages of phase-field models are underlined.~~

Keywords: Phase-field, Fracture mechanics, Variational formulation, Brittle fracture, Isogeometric Analysis

---

1. Introduction

~~So as to~~ shorten development times, the prediction of fracture and failure in materials play a significant role for engineering designs. Mostly, experiments are not profitable due to high expense and enormous costs. So as to overcome these problems, computational models have been proposed in order to accurately model theses physical effects.

Finite Element Methods (FEM) are commonly used to numerically approximate crack behaviour in a given context. ~~Here,~~ a robust and efficient implementation is to the fore. A major question arising while modelling fracture processes within the FEM context is how to describe the splitting of the material. ~~Obviously,~~ it is not possible to simply let connected Finite Elements be separated from one point in time to the other. ~~Thus, so called~~ *sharp interface models* have been proposed by enriching the displacement field with discontinuities

---

or by inserting discontinuities by means of mesh handling. ~~So as to~~ give a short introduction to these approaches, subsequently, two of them are sketched. ~~Since these kind of strategies are not topic of this work, it is referred to Appendix A where they are explained in a bit more detail.~~

The *virtual crack closure technique* represents a crack by introducing one-dimensional discontinuities by a line of nodes. So as to let several Finite Elements separate from each other, there exist nodes with identical coordinates. If a crack forms, these nodes can move apart from each other. In the case of undamaged material, multipoint constraints are imposed on these nodes so that they behave in the same manner. [20]

In the *cohesive segments method* the crack is represented by a set of overlapping cohesive segments. By means of these segments, displacement jumps are introduced as soon as the current stress state violates a given fracture criterion. However, this approach leads to several disadvantages: Quadrature rules have to be adapted, nodes need to have a variable number of degrees of freedom, there is a high accuracy error, the stress state at the tip of a segment is not well described and the specification of the geometry of the cohesive surfaces might lead to problems. [29][30]

~~However,~~ extending these formulations to three dimensions has proven to be difficult. ~~Thus, today~~ many approaches base on the variational formulation of brittle fracture. Francfort and Marigo [14] propose that the solution of the fracture problem based on Griffith's theory is given by the minimizer of a global energy functional. In Griffith's theory, a critical energy release rate determines crack nucleation and propagation. Accuracy and robustness of the variational formulation in two and three dimensions using the so called *phase-field methods* have been shown for instance by Miehe et al. [23] and Miehe et al. [26]. In there, a derivation of the phase-field based on continuum mechanics and thermodynamics is presented. Additionally, in [23] the model distinguishing between tensile and compressive effects on crack growth has been established. Successful extensions to dynamic problems have been given by Borden et al. [8], Bourdin et al. [11], Hofacker and Miehe [16], Larsen [21] and Larsen et al. [22]. For example, Karma et al. [19] do not base their dynamic phase-field formulation on Griffith's theory of brittle fracture. However, this paper only deals with Griffith's theory as used for example by Bourdin et al. [10] since this theory is well understood and it has been proven to be useful in engineering applications [8]. The established phase-field models using the variational formulation of fracture have been widely numerically used and proved in different engineering contexts, for instance by Bourdin et al. [9] and Mikelić et al. [27] for hydraulic fracturing, by Wilson and Borden [32] for piezoelectric ceramics, by Miehe and Schänzel [24] for rubbery polymers and by Miehe et al. [25] for thermo-elastic solids. All these examples outline the relevance and the attractiveness of this formulation. In fact, for example Borden et al. [6] have shown that the phase-field method can also be used so as to model ductile fracture. ~~Nevertheless,~~ this work focuses on brittle fracture. ~~A basic derivation of the governing equations considering ductile fracture is given in Appendix B.~~

In general, *phase-field methods* are used so as to model interfaces between regions of different phases. Examples are the modelling of solidification behaviour, interfaces between fluids with different properties or, as discussed in this work, fracture. In the latter case, the interface describes the region between undamaged and totally broken material. Within

the brittle fracture context, the phase-field theory can be seen as a regularization of the mentioned variational formulation. In there, the abrupt change between elastic behaviour and crack nucleation is smoothed as well as the boundary between undamaged and damaged material. ~~Thus, no discontinuities are introduced into the body and~~ the transition between two different phases is smoothed as it happens in a diffusive process. That is why the phase-field method belongs to the so called *diffuse interface models.*

~~Isogeometric Analyis (IGA) is a powerful method in which functions used for the description of Computer Aided Design (CAD) geometries are adopted as a basis for analysis.~~ Within the FEM context, ~~no mesh generation is required~~ and IGA allows for a high global regularity of the numerical solution. Especially, as soon as C^2-continuity is required, standard Finite Elements quickly reach their beneficial properties. The IGA-framework has been established by Hughes et al. [17]. The main concept lies in the usage of ~~B-splines~~ so as to model a geometry or, within the FEM context, in order to get a higher regularity using these functions as ~~ansatz functions~~. The introduction of hierarchical B-Splines by Forsey and Bartels [13] has offered the possibility of local refinement. This approach has been expanded to the local refinement of NURBS (Non-Uniform Rational B-Splines). Sederberg et al. [31] have introduced so called T-Splines for the sake of a more efficient discretization of surfaces in contrast to hierarchical B-Splines. Local refinement strategies for these have been established as well as for NURBS, so called LR NURBS (Locally Refined NURBS) [33].

There exist many publications on fracture computations within an IGA framework. Just to mention two, Irzal et al. [18] have developed an interface element based on IGA in the context of a sharp interface model of fracture and Quoc Bui et al. [28] have made use of an extended IGA (XIGA) framework for the sake of modelling dynamic fracture in multiphase piezoelectric/piezomagnetic composites. In [5], results of several papers concerning phase-field methods of dynamic fracture within an IGA framework are summarized. In there and in the corresponding papers [6][7][8], it has been observed that this complete framework works well for complex crack patterns and nucleation, even in three dimensions. By reason of a proposed higher order model, the used IGA framework by Hughes et al. [17] has been proven to be very beneficial so as to achieve higher regularity in the numerical solution. In [8], an adaptive refinement strategy using T-Splines has been proposed and numerically investigated.

In this work, ~~firstly,~~ the governing equations for obtaining stress equilibrium and for modelling the evolution of the phase-field are derived (Section 2). In there, brittle fracture is considered and its variational formulation is outlined. Its minimizer is found by solving the Euler-Lagrange equation. At the end of Section 2, shortly, differences in modelling ductile fracture in contrast to brittle fracture are pointed out. Since this works focuses on brittle fracture, a detailed derivation of the governing equations for this type of fracture can be found in Appendix B. Section 3 focuses on the approximation of the solution of the governing equations including the derivation of the weak and semidiscrete Galerkin forms. Shortly, a motivation for using an IGA framework so as to numerically solve these forms is given. Additionally, an appropriate time integration scheme for the given problem is outlined. This work finishes with Section 4 by summarizing the phase-field model of dynamic

fracture. Especially, phase-field methods of fracture are compared to sharp interface models of fracture so as to highlight the advantages of diffuse interface models for this type of problems.

2. Phase-field formulation

The phase-field model as a diffuse interface model does not introduce discontinuities into the solid but the fracture surface is approximated by a scalar valued field. Thus, the boundary between damaged and undamaged regions is smoothed. In the following parts, a model for brittle fracture as well as a second- and fourth-order model are presented. At first, the notation and formulation considering brittle fracture is introduced. Since this work focuses on brittle fracture, at the end of this section, differences in the formulation considering ductile fracture are outlined. A more detailed derivation of the governing equations considering ductile fracture can be found in Appendix B.

For the rest of this paper, following notation is made (see Fig. 1(a)). The arbitrary body $\Omega \subset \mathbb{R}^d$ ($d \in \{1, 2, 3\}$) has external boundary $\partial\Omega$ and evolving internal discontinuity boundary Γ (fracture surface). The displacement field at a given point $\mathbf{x}$ and time t is given by $\mathbf{u}(\mathbf{x}, t) \in \mathbb{R}^d$. Dirichlet boundary conditions $\mathbf{u}(\mathbf{x}, t) = \mathbf{g}(\mathbf{x}, t)$ on $\partial\Omega_{\mathbf{g}}$ and Neumann boundary conditions $\mathbf{t}(\mathbf{x}, t) = \mathbf{h}(\mathbf{x}, t)$ on $\partial\Omega_{\mathbf{h}}$ are imposed with $\partial\Omega_{\mathbf{g}} \cup \partial\Omega_{\mathbf{h}} = \partial\Omega$. $\mathbf{t}(\mathbf{x}, t)$ describes a given traction vector force.
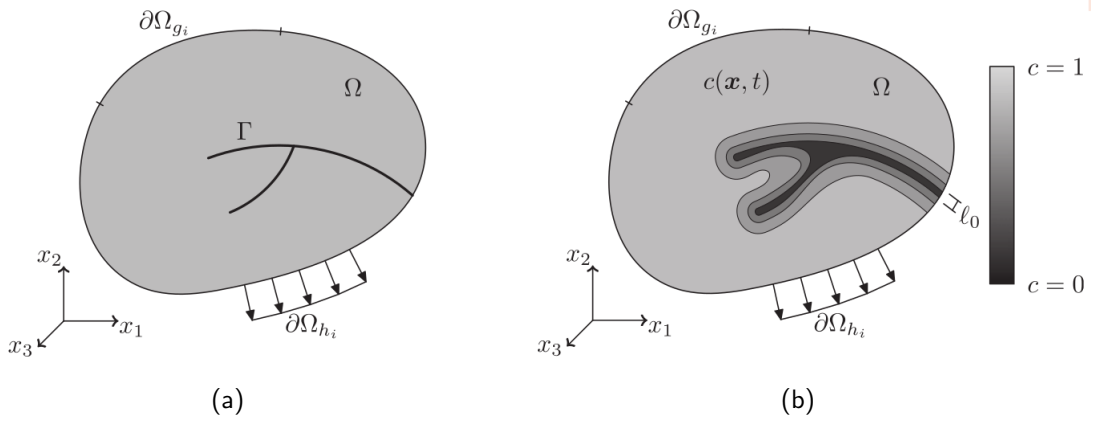

Fig. 1. (a) Representation of a solid body Ω and internal discontinuitiy boundary Γ. (b) Phase-field approximation of Γ. $c(\mathbf{x}, t)$ describes the phase-field and l_0 is a parameter controlling the failure zone's width. [8]

2.1. Griffith's theory of brittle fracture

Considering small deformations and deformation gradients, the small strain tensor $\boldsymbol{\varepsilon}(\mathbf{x}, t)$ is given by

$$\boldsymbol{\varepsilon} = \nabla^s \mathbf{u} \tag{1}$$

where $(\cdot)^s$ refers to the symmetric part. Considering isotropic linear elasticity, the undamaged elastic energy density can be expressed by

$$\Psi_e(\boldsymbol{\varepsilon}) = \frac{1}{2}\lambda tr(\boldsymbol{\varepsilon})^2 + \mu\boldsymbol{\varepsilon} : \boldsymbol{\varepsilon} \tag{2}$$

4

using the Lamé constants λ and μ and $(\cdot) : (\cdot)$ denoting the double contraction.

According to the energetic approaches to fracture, the critical fracture energy density $\mathcal{G}_c$ defines the energy being necessary to create a unit area of fracture surface. Since translation of cracks shall be forbidden but extension, branching and merging shall be allowed, there is an irreversibility condition stating that $\Gamma(t) \subseteq \Gamma(t + \Delta t), \forall \Delta t > 0$.

However, Griffith's fracture theory reaches its limits as soon as it is used to predict crack paths, nucleation of new cracks and complicated crack behaviours during kinking and branching. Thus, the problem is formulated in a variational sense which is shown in the following paragraphs. The phase-field approach can then be seen as a regularized version of this variational formulation. [4]

Newton's laws follow Hamilton's principle stating that the functional

$$J(q, \dot{q}) = \int_{t_0}^{t_1} \mathcal{L}(q, \dot{q}, t)\, \mathrm{d}t \tag{3}$$

reaches a stationary point. $\mathcal{L}(q, \dot{q}, t)$ describes the so called Lagrangian and q represents generalized coordinates. The motion of the mechanical system from t_0 to t_1 is then captured by this formulation [15]. In the case presented here, the Lagrangian reads $\mathcal{L}(\mathbf{u}, \dot{\mathbf{u}}, \Gamma) = \Psi_{kin}(\mathbf{u}) - \Psi_{pot}(\mathbf{u}, \Gamma)$. Inserting the introduced critical fracture energy density $\mathcal{G}_c$, the kinetic energy of the body and (2) leads to

$$\mathcal{L}(\mathbf{u}, \dot{\mathbf{u}}, \Gamma) = \int_{\Omega} \left(\frac{1}{2} \rho \dot{\mathbf{u}} \dot{\mathbf{u}} - \Psi_e(\boldsymbol{\varepsilon}) \right) \mathrm{d}\Omega - \int_{\Gamma} \mathcal{G}_c \mathrm{d}\Gamma. \tag{4}$$

The Euler-Lagrange Equation (ELE) is a differential equation whose solution satisfies the required equilibrium. Thus, this equation is also called the equation of motion[1]. A minimizer q of (4) satisfies the ELE

$$\frac{\partial \mathcal{L}}{\partial q} - \frac{\mathrm{d}}{\mathrm{d}t} \frac{\partial \mathcal{L}}{\partial \dot{q}} = 0. \tag{5}$$

For a given $\mathcal{L} = \mathcal{L}(q, \dot{q}, \ddot{q}, t)$ this differential equation changes to

$$\frac{\partial \mathcal{L}}{\partial q} - \frac{\mathrm{d}}{\mathrm{d}t} \frac{\partial \mathcal{L}}{\partial \dot{q}} + \frac{\mathrm{d}^2}{\mathrm{d}t^2} \frac{\partial \mathcal{L}}{\partial \ddot{q}} = 0 \tag{6}$$

[15]. In (4), the fracture surface Γ has to be known so as to evaluate this expression. Since this discontinuity is propagating, high computational costs have to be accepted so as to algorithmically track the propagating surface. So as to circumvent this, the *phase-field* approach, which regularizes the just mentioned variational formulation, has been introduced. This will be presented in the next chapters.

---

[1]The term *equation of motion* may be a bit misleading. It refers to the differential equation and not to its solution.

2.2. Phase-field theory

As can be seen in Fig. 1(b) the fracture surface Γ is approximated by a scalar valued field $c(\mathbf{x}, t)$. This field is called the *phase-field*. Values of $c = 1$ represent regions away from the crack (undamaged material) whereas $c = 0$ indicates totally broken material (at $c = 0$, there is a crack). Now, in (4) the surface integral and thus, the need for tracking the crack can be eliminated. The approximation reads as follows:

$$\int_\Gamma \mathcal{G}_c \mathrm{d}\Gamma \approx \int_\Omega \mathcal{G}_c \Gamma_{c,n} \mathrm{d}\Omega. \tag{7}$$

Obviously, the surface integral can now be approximately calculated without knowing or tracking the fracture surface. (7) represents the fracture surface energy. The quantity $\Gamma_{c,n}$ is called the crack density functional which depends on a parameter l_0, the phase-field $c(\mathbf{x}, t)$ and its spatial derivatives up to order $\frac{n}{2}$ ($\frac{\partial c}{\partial \mathbf{x}}, .., \frac{\partial^{\frac{n}{2}} c}{\partial \mathbf{x}^{\frac{n}{2}}}$) with n being an even number. $l_0 \in \mathbb{R}^+$ represents a parameter controlling the width of the approximation of the crack (see Fig. 1(b)). It could be seen as a numerical regularization parameter or as an material parameter. Borden et al. [8] showed that a critical stress level σ_c depends on l_0. Thus, here, this parameter is here seen as a material property. For a more detailed discussion it is referred to the investigations of Amor et al. [3].

The notation $\Gamma_{c,n}$ already presages that n determines the order of the approximation. Borden et al. [7] have presented a so called *second-* and *fourth-order phase-field theory*. For $n = 2$, the crack density functional introduced by Bourdin et al. [10] is used whereas for $n = 4$, a new functional has been established:

$$
\begin{aligned}
\Gamma_{c,2} &= \frac{1}{4l_0} \left[(c - 1)^2 + 4l_0^2 |\nabla c|^2 \right], \\
\Gamma_{c,4} &= \frac{1}{4l_0} \left[(c - 1)^2 + 2l_0^2 |\nabla c|^2 + l_0^4 (\Delta c)^2 \right].
\end{aligned}
\tag{8}
$$

These formulations have been analytically analysed. So as to keep things short, it is referred to the work by Borden et al. [7] for more detailed information. Only one important aspect is mentioned here: $(8)_1$ is well-posed variationally for all $c \in H^1(\Omega)$ and solutions will generally not show greater regularity. Thus, $(8)_2$ has been introduced so as to provide higher regularity in the solutions.

2.3. Energy approximation

In the failure zone, there is a loss of material stiffness. So as to model this phenomenon, the elastic energy is split into contributions from tensile and compressive deformations[2]

$$\Psi_e(\boldsymbol{\varepsilon}, c) = g(c) \Psi_e^+(\boldsymbol{\varepsilon}) + \Psi_e^-(\boldsymbol{\varepsilon}) \tag{9}$$

---

[2]Originally, a parameter k or $\eta \ll 1$ has been introduced by Ambrosio and Tortorelli [2] into this equation so as to avoid ill-posedness. However, Borden et al. [8] have found out that there is no necessity of setting $k > 0$. Thus, the derivation of the governing evolution equations all consider the case $k \equiv 0$.

with the so called degradation function $g(c)$. In [8], $g(c) = c^2$ has been used. Nevertheless, in [6] it has been examined that this quadratic function is not leading to a linear stress-strain-curve up to the point of critical stress. To overcome this problem, Borden et al. [6] propose the following parametrized cubic degradation function:

$$g(c) = m(c^3 - c^2) + 3c^2 - 2c^3 \tag{10}$$

with $m > 0$ determining the slope of g at $c = 1$. This cubic degradation function leads to $\sigma = E\varepsilon$ as $m \to 0$ for strains up to the critical strain considering the quadratic degradation function. Thus, $m = 10^{-4}$ has been chosen in their numerical examples. The two major accomplishments using the cubic degradation function are at first, the nearly linear stress-strain behaviour up to the point of critical stress. Thus, linear elasticity is modelled more accurately. Secondly, it shows up that the critical stress is higher than the one considering the quadratic degradation function (for l_0 fixed). Thus, a larger length scale parameter can be used so as to achieve the critical stress since $\sigma_{crit}^{cubic} \sim l_0^{-\frac{1}{2}}$. As a consequence, coarser meshes can be used in order to reduce computational effort. However, in the following only the function $g(c)$ is used so as to keep the derivation more generic. The splitting in (9) is achieved with the help of spectral decomposition of the strain:

$$\boldsymbol{\varepsilon} = \mathbf{P}\boldsymbol{\Lambda}\mathbf{P}^T \quad \Rightarrow \quad \boldsymbol{\varepsilon}^+ = \mathbf{P}\boldsymbol{\Lambda}^+\mathbf{P}^T, \ \boldsymbol{\varepsilon}^- = \mathbf{P}\boldsymbol{\Lambda}^-\mathbf{P}^T,$$

$$\boldsymbol{\Lambda}^+ = diag(\langle\lambda_1\rangle, \langle\lambda_2\rangle, \langle\lambda_3\rangle), \quad \langle x \rangle = \begin{cases} x, & x > 0 \\ 0, & x \leq 0 \end{cases}. \tag{11}$$

$\boldsymbol{\Lambda}^-$ is analogously defined. $\lambda_i \in \sigma(\boldsymbol{\varepsilon}), i \in \{1,2,3\}$ denote the eigenvalues of the strain tensor. Plugging (11) into (2) leads to the energy contributions from tensile and compressive deformations:

$$\Psi_e^+(\boldsymbol{\varepsilon}) = \frac{1}{2}\lambda\langle tr(\boldsymbol{\varepsilon})\rangle^2 + \mu tr\left[(\boldsymbol{\varepsilon}^+)^2\right],$$

$$\Psi_e^-(\boldsymbol{\varepsilon}) = \frac{1}{2}\lambda(tr(\boldsymbol{\varepsilon}) - \langle tr(\boldsymbol{\varepsilon})\rangle)^2 + \mu tr\left[(\boldsymbol{\varepsilon} - \boldsymbol{\varepsilon}^+)^2\right]. \tag{12}$$

The assumption here is that the sign of the principal strains determine tensile and compressive contributions. Putting (9) and (7) together leads to the Helmholtz free energy:

$$\Psi_n = g(c)\Psi_e^+ + \Psi_e^- + \mathcal{G}_c\Gamma_{c,n}. \tag{13}$$

2.4. Strong form

The governing equations will include one for enforcing stress equilibrium and the other will govern the evolution of the phase-field.

Assuming given body forces $\mathbf{b}$ and traction vector forces $\mathbf{t} = \boldsymbol{\sigma}\mathbf{n}$ with outward-pointing

normal vector $\mathbf{n}$ on $\partial\Omega$, stress equilibrium is enforced by

$$
\begin{cases}
\nabla \cdot \boldsymbol{\sigma} + \mathbf{b} = \rho\ddot{\mathbf{u}} & \text{on } \Omega \times (0, T) \\
\mathbf{u} = \mathbf{g} & \text{on } \partial\Omega_{\mathbf{g}} \times (0, T) \\
\boldsymbol{\sigma}\mathbf{n} = \mathbf{h} & \text{on } \partial\Omega_{\mathbf{h}} \times (0, T) \\
\mathbf{u} = \mathbf{u}_0 & \text{on } \Omega \times 0 \\
\dot{\mathbf{u}} = \mathbf{v}_0 & \text{on } \Omega \times 0.
\end{cases}
\tag{14}
$$

$(14)_1$ represents the local form of the linear momentum balance with $\boldsymbol{\sigma} = g\left(c\right)\frac{\partial\Psi_e^+}{\partial\boldsymbol{\varepsilon}} + \frac{\partial\Psi_e^-}{\partial\boldsymbol{\varepsilon}}$.

As described in Section 2.1, the Euler-Lagrange Equation can be used to find a minimizer of (3). Plugging (8) and (9) into (4) as well as using (7) makes the use of the ELE possible. For this case, $q\,\hat{=}\,c$ and $\frac{\mathrm{d}}{\mathrm{d}t}\,\hat{=}\,\frac{\mathrm{d}}{\mathrm{d}\mathbf{x}}$. All this together leads to the governing equations for the evolution of the phase-field, namely $(16)_1$ for the second- and $(17)_1$ for the fourth-order phase-field theory. As can be seen in these equations, Ψ_e^+ has been replaced by the strain history field $\mathcal{H}$ enforcing the irreversibility condition $\Gamma\left(t\right) \subseteq \Gamma\left(t + \Delta t\right), \forall \Delta t > 0$ in the strong form. This field satisfies the Kuhn-Tucker conditions for loading and unloading [8]:

$$
\Psi_e^+ - \mathcal{H} \leq 0, \quad \dot{\mathcal{H}} \geq 0, \quad \dot{\mathcal{H}}\left(\Psi_e^+ - \mathcal{H}\right) = 0.
\tag{15}
$$

In the work of Miehe et al. [23] a detailed motivation for the introduction of this field can be found. It can also be used to model pre-existing cracks or geometrical features [8].

As a result, the strong forms of the governing equations for the phase-field's evolution are given by:

n=2:

$$
\begin{cases}
\dfrac{2l_0\mathcal{H}}{\mathcal{G}_c}g'\left(c\right) + c - 4l_0^2\Delta c = 1 & \text{on } \Omega \times (0, T) \\
\nabla c \cdot \mathbf{n} = 0 & \text{on } \partial\Omega \times (0, T) \\
c = c_0 & \text{on } \Omega \times 0
\end{cases}
\tag{16}
$$

n=4:

$$
\begin{cases}
\dfrac{2l_0\mathcal{H}}{\mathcal{G}_c}g'\left(c\right) + c - 2l_0^2\Delta c + l_0^4\Delta\left(\Delta c\right) = 1 & \text{on } \Omega \times (0, T) \\
\Delta c = 0 & \text{on } \partial\Omega \times (0, T) \\
\nabla\left(l_0^4\Delta c - 2l_0^2 c\right) \cdot \mathbf{n} = 0 & \text{on } \partial\Omega \times (0, T) \\
c = c_0 & \text{on } \Omega \times 0
\end{cases}
\tag{17}
$$

with the derivative $g'\left(c\right)$ of the used degradation function (see (10)). The boundary conditions on the phase-field result from the homogeneous natural boundary conditions arising from the derivation of the weak form [5]. The numerical approximation of the solutions of (16) and (17) are outlined in Section 3. The following section reveals the differences in modelling ductile fracture in contrast to brittle fracture which has been considered up to this point.

8

2.5. Ductile fracture

In this section, the differences between models of brittle and ductile fracture are examined. Up to this point of this paper, linear elasticity has been assumed. In this context, brittle fracture has been formulated in a variational way. By introducing the phase-field approximation, a regularized formulation of the variational one has been established. The corresponding stress-strain-curves and the procedure are illustrated in Fig. 2.
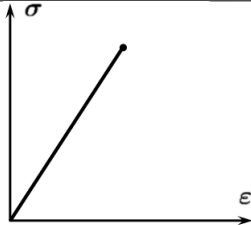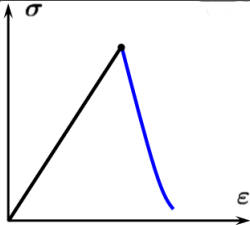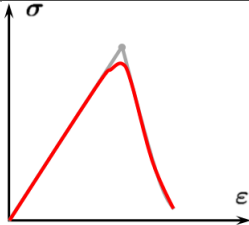
Linear elasticity	Brittle fracture	
$E(\mathbf{u})$	Variational formulation of brittle fracture $E(\mathbf{u}, \Gamma)$	Phase-field formulation ($\hat{=}$regularized version) $E(\mathbf{u}, c)$

Fig. 2. Brittle fracture: Process from linear elasticity over the variational formulation towards the phase-field approximation. Note that $E(\mathbf{u})$ refers to the integral of the elastic energy density Ψ_e over the body Ω: $E(\mathbf{u}) = \int_\Omega \Psi_e(\varepsilon(\mathbf{u})) \, \mathrm{d}\Omega$. [1]
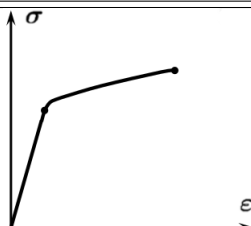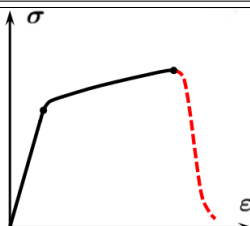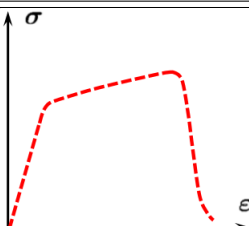
Plasticity	Ductile fracture	
$E(\varepsilon^e, \varepsilon^p, \alpha)$	Variational formulation of ductile fracture $E(\varepsilon^e, \varepsilon^p, \alpha, \Gamma)$	Phase-field formulation ($\hat{=}$regularized version) $E(\varepsilon^e, \varepsilon^p, \alpha, c)$

Fig. 3. Ductile fracture: Process from plasticity towards the phase-field approximation. The variational formulation has not been established yet. As before, $E(\varepsilon^e, \varepsilon^p, \alpha)$ refers to the integral of the energy density over the body Ω, for example considering the J_2-plasticity framework: $E(\varepsilon^e, \varepsilon^p, \alpha) = \int_\Omega [\Psi_e(\varepsilon^e) + \Psi_p(\alpha)] \, \mathrm{d}\Omega$. [1]

The variational formulation has been well established. Thus, the regularized version using the phase-field approximation could be found. As the dashed lines in Fig. 3 reveal, there is no variational formulation of ductile fracture found yet. Thus, the foundation of the regularized version is not as straightforward as for brittle fracture. So as to circumvent this problem, the derivation of the governing equations considering ductile fracture are based on microforces and balance laws. So as to keep the focus of this work on brittle fracture, the derivation can be found in Appendix B. Note that the governing equations for brittle fracture could also have been derived using the approach based on the balance laws, especially the microforce balance. For a more detailed derivation, it is referred to [5].

3. Numerical formulation

Formulas (14) and (16) or (17), respectively, represent the strong form of the given problem. As throughout this work, brittle fracture is considered and the weak form is derived. Subsequently, an Isogeometric Analysis framework as well as a time integration scheme is presented.

3.1. Weak and semidiscrete Galerkin form

For the derivation of the weak form, at first, suitable function spaces have to be defined:

$$
\begin{aligned}
\boldsymbol{\mathcal{S}} &= \{\mathbf{u}(t) \in \left(H^1(\Omega)\right)^d | \mathbf{u}(t) = \mathbf{g} \text{ on } \partial\Omega_{\mathbf{g}}\}, \\
\boldsymbol{\mathcal{V}} &= \{\mathbf{w} \in \left(H^1(\Omega)\right)^d | \mathbf{u}(t) = \mathbf{0} \text{ on } \partial\Omega_{\mathbf{g}}\}, \\
\tilde{\mathcal{S}}_n &= \{c(t) \in H^{\frac{n}{2}}(\Omega)\}, \\
\tilde{\mathcal{V}}_n &= \{q \in H^{\frac{n}{2}}(\Omega)\}.
\end{aligned}
\tag{18}
$$

So as to obtain the weak form, the governing equations have to be multiplied with testing functions, the divergence theorem has to be applied and boundary conditions need to be plugged in. Taking the testing functions from the spaces $\boldsymbol{\mathcal{V}}$ and $\tilde{\mathcal{V}}_n$, respectively, leads to the following weak forms for the second- and fourth-order phase-field theory for brittle fracture:

n=2: Find $\mathbf{u}(t) \in \boldsymbol{\mathcal{S}}$ and $c(t) \in \tilde{\mathcal{S}}_2, t \in [0, T]$ so that $\forall \mathbf{w} \in \boldsymbol{\mathcal{V}}$ and $\forall q \in \tilde{\mathcal{V}}_2$:

$$
\begin{cases}
(\rho\ddot{\mathbf{u}}, \mathbf{w})_\Omega + (\boldsymbol{\sigma}, \nabla\mathbf{w})_\Omega = (\mathbf{h}, \mathbf{w})_{\partial\Omega_{\mathbf{h}}} + (\mathbf{b}, \mathbf{w})_{\partial\Omega_{\mathbf{g}}} \\
\left(\dfrac{2l_0\mathcal{H}}{\mathcal{G}_c}g'(c) + c, q\right)_\Omega + \left(4l_0^2\nabla c, \nabla q\right)_\Omega = (1, q)_\Omega \\
(\rho\mathbf{u}(0), \mathbf{w})_\Omega = (\rho\mathbf{u}_0, \mathbf{w})_\Omega \\
(\rho\dot{\mathbf{u}}(0), \mathbf{w})_\Omega = (\rho\dot{\mathbf{u}}_0, \mathbf{w})_\Omega \\
(c(0), q)_\Omega = (c_0, q)_\Omega
\end{cases}
\tag{19}
$$

n=4: Find $\mathbf{u}(t) \in \boldsymbol{\mathcal{S}}$ and $c(t) \in \tilde{\mathcal{S}}_4, t \in [0, T]$ so that $\forall \mathbf{w} \in \boldsymbol{\mathcal{V}}$ and $\forall q \in \tilde{\mathcal{V}}_4$:

$$\begin{cases} (\rho \ddot{\mathbf{u}}, \mathbf{w})_\Omega + (\boldsymbol{\sigma}, \nabla \mathbf{w})_\Omega = (\mathbf{h}, \mathbf{w})_{\partial\Omega_\mathbf{h}} + (\mathbf{b}, \mathbf{w})_{\partial\Omega_\mathbf{g}} \\ \left(\dfrac{2l_0 \mathcal{H}}{\mathcal{G}_c} g'(c) + c, q\right)_\Omega + \left(2l_0^2 \nabla c, \nabla q\right)_\Omega + \left(l_0^4 \Delta c, \Delta q\right)_\Omega = (1, q)_\Omega \\ (\rho \mathbf{u}(0), \mathbf{w})_\Omega = (\rho \mathbf{u}_0, \mathbf{w})_\Omega \\ (\rho \dot{\mathbf{u}}(0), \mathbf{w})_\Omega = (\rho \dot{\mathbf{u}}_0, \mathbf{w})_\Omega \\ (c(0), q)_\Omega = (c_0, q)_\Omega \end{cases} \tag{20}$$

with $(\cdot, \cdot)_\Omega$ denoting the inner product with respect to the L^2-norm.

So as to solve problems (19) and (20), it is necessary to choose finite-dimensional sub-spaces to the function spaces mentioned in (18). Let $\boldsymbol{\mathcal{S}}^h \subset \boldsymbol{\mathcal{S}}$, $\boldsymbol{\mathcal{V}}^h \subset \boldsymbol{\mathcal{V}}$, $\tilde{\mathcal{S}}_n^h \subset \tilde{\mathcal{S}}_n$, $\tilde{\mathcal{V}}_n^h \subset \tilde{\mathcal{V}}_n$ and let $N_A(\mathbf{x})$ denote the shape functions within the Finite Element approximation. Furthermore, the required functions within an element (with n_{nodes} denoting the number of nodes per element) are approximated as linear combinations of these shape functions:

$$\begin{aligned} \mathbf{u}(\mathbf{x}, t) \approx \mathbf{u}^h(\mathbf{x}, t) &= \sum_{A=1}^{n_{\text{nodes}}} N_A(\mathbf{x}) \mathbf{u}_A(t), \\ \mathbf{w}(\mathbf{x}, t) \approx \mathbf{w}^h(\mathbf{x}, t) &= \sum_{A=1}^{n_{\text{nodes}}} N_A(\mathbf{x}) \mathbf{w}_A(t), \\ c(\mathbf{x}, t) \approx c^h(\mathbf{x}, t) &= \sum_{A=1}^{n_{\text{nodes}}} N_A(\mathbf{x}) c_A(t), \\ q(\mathbf{x}, t) \approx q^h(\mathbf{x}, t) &= \sum_{A=1}^{n_{\text{nodes}}} N_A(\mathbf{x}) q_A(t). \end{aligned} \tag{21}$$

In order to obtain the semidiscrete Galerkin form of the problem, these approximations $(\cdot)(\mathbf{x}, t) \approx (\cdot)^h(\mathbf{x}, t)$ have to be plugged in into (19) and (20). Changing the function spaces in these formulations and inserting (21) will lead to the semidiscrete Galerkin form. These forms are not shown explicitly here due to the fact that only the superscript $(\cdot)^h$ has to be written next to the functions and function spaces. Apart from that, they are identical to the weak forms. Note that for the cubic degradation function (10), the first term in both, the second- and fourth-order phase-field evolution equation, needs to be linearized. Since the phase-field is only scalar-valued, the linearization around c_0 is straight-forward:

$$\begin{aligned} g'(c) &= m\left(3c^2 - 2c\right) + 6c - 6c^2, \\ g'_{lin}(c) &= m\left(3\left(c_0^2 + 2c_0(c - c_0)\right) - 2c\right) + 6c - 6\left(c_0^2 + 2c_0(c - c_0)\right). \end{aligned} \tag{22}$$

$c_0 = 0$??

Γ-convergence has already been shown for the second-order phase-field theory but it has not been proved for the fourth-order theory yet. However, Borden et al. [7] have showed that the latter is well behaved in numerical examples. Comments on existing results of the higher-order model will shortly be outlined in Section 4.

3.2. Spatial discretization

Regarding the governing equation of the phase-field's evolution for the fourth-order phase-field theory $(20)_2$, the term Δc reveals that the numerical solution of the phase-field c needs to be globally twice continuous differentiable. Within the Finite Element context, this leads to a significant problem. Since in general, standard Finite Element Analysis is based on a continuous but not a smooth basis, the solutions are not globally twice continuous differentiable so that the term Δc on Ω would not be well-defined. As a consequence, the traditional Finite Elements cannot be used within this context. Using Isogeometric Finite Elements can circumvent this problem. Isogeometric Analysis (IGA) allows for an exact representation of geometries, even spherical or cylindrical shapes can be represented exactly which is not possible using standard Finite Elements. In general, the isogeometric basis is smooth which overcomes the problem of the necessity of a higher regularity. As an additional benefit, it leads to a more accurate stress representation [8].

As already described in Section 1, the main idea is to use the same basis for both, the analysis and the description of the model's geometric domain. Herefore, B-Splines, non-uniform rational B-Splines (NURBS) or T-Splines are used so as to compute with a smooth basis. The function approximations (21) stay the same. Only the shape functions N_A differ from classical Finite Element Analysis. Since CAD geometries are based on NURBS, mesh changes like local refinements preserve the exact CAD geometry and no mapping between CAD geometry and FE geometry has to be established. [5]

Especially, recent works like [33] provide a mechanism for the local refinement of the splines used in IGA. Local refinement is surely necessary so as to resolve and capture complex crack patterns in detail and in order to achieve accurate numerical results [8].

3.3. Time discretization

Since this work deals with dynamic fracture, there is a need for an appropriate time integration scheme. Here, a monolithic generalized-α method is presented. This implicit method has been proposed by Chung and Hulbert [12] in 1993. Advantages of this method are its second order accuracy as well as unconditonal stability provided that the parameters are well chosen. The notation used here is taken from the work of Borden et al. [7] and Borden et al. [8], respectively.

On the basis of $(19)_1$, $(20)_1$ and (21), let the residual vectors for the displacement be defined as

$$
\begin{aligned}
\mathbf{R}^u &= \{R^u_{A,i}\}, \\
R^u_{A,i} &= (\mathbf{h}, N_A\mathbf{e}_i)_{\partial\Omega_{\mathbf{h}}} + (\mathbf{b}, N_A\mathbf{e}_i)_{\partial\Omega_{\mathbf{g}}} - \left(\rho\ddot{\mathbf{u}}^h, N_A\mathbf{e}_i\right)_\Omega - \left(\sigma_{jk}, B^{ijk}_A\right)_\Omega,
\end{aligned}
\tag{23}
$$

with i'th Euclidean basis vector $\mathbf{e}_i$ and

$$
B^{ijk}_A = \frac{1}{2}\left(\frac{\partial N_A}{\partial x_j}\delta_{ik} + \frac{\partial N_A}{\partial x_k}\delta_{ij}\right)
\tag{24}
$$

so that $\epsilon_{ijk} = \sum_A B^{ijk}_A u_{A,i}$.

For the second-order phase-field theory of brittle fracture, the residual vectors based on $(19)_2$ are given by

$$\mathbf{R}^c = \{R_A^c\},$$
$$R_A^c = (1, N_A)_\Omega - \left(\frac{2l_0 \mathcal{H}}{\mathcal{G}_c} g'_{lin}(c^h) + c^h, N_A\right)_\Omega - \left(4l_0^2 c_{,i}^h, N_{A,i}\right)_\Omega. \tag{25}$$

For the fourth-order phase-field theory of brittle fracture, these residual vectors based on $(20)_2$ change to:

$$\mathbf{R}^c = \{R_A^c\},$$
$$R_A^c = (1, N_A)_\Omega - \left(\frac{2l_0 \mathcal{H}}{\mathcal{G}_c} g'_{lin}(c^h) + c^h, N_A\right)_\Omega - \left(2l_0^2 c_{,i}^h, N_{A,i}\right)_\Omega - \left(l_0^4 c_{,ii}^h, N_{A,jj}\right)_\Omega. \tag{26}$$

Considering time step n, time step size $\Delta t = t_{n+1} - t_n$, parameters $\alpha_f, \alpha_m, \beta, \gamma$ as well as vectors $\mathbf{u}_n$ and $\mathbf{c}_n$ for the control variable degrees-of-freedom of the displacements and phase-field (see (21)), $\mathbf{v}_n := \dot{\mathbf{u}}_n$ and $\mathbf{a}_n := \ddot{\mathbf{u}}_n$ are defined. Using this notation, the method reads as follows:

Given $\mathbf{u}_n$, $\mathbf{v}_n$ and $\mathbf{a}_n$. Find $\mathbf{u}_{n+1}$, $\mathbf{v}_{n+1}$, $\mathbf{a}_{n+1}$, $\mathbf{u}_{n+\alpha_f}$, $\mathbf{v}_{n+\alpha_f}$, $\mathbf{a}_{n+\alpha_m}$ and $\mathbf{c}_{n+1}$ so that:

$$
\begin{aligned}
\mathbf{R}^u\left(\mathbf{u}_{n+\alpha_f}, \mathbf{v}_{n+\alpha_f}, \mathbf{a}_{n+\alpha_m}, \mathbf{c}_{n+1}\right) &= 0, \\
\mathbf{R}^c\left(\mathbf{u}_{n+\alpha_f}, \mathbf{c}_{n+1}\right) &= 0, \\
\mathbf{u}_{n+\alpha_f} &= \mathbf{u}_n + \alpha_f\left(\mathbf{u}_{n+1} - \mathbf{u}_n\right), \\
\mathbf{v}_{n+\alpha_f} &= \mathbf{v}_n + \alpha_f\left(\mathbf{v}_{n+1} - \mathbf{v}_n\right), \\
\mathbf{a}_{n+\alpha_m} &= \mathbf{a}_n + \alpha_m\left(\mathbf{a}_{n+1} - \mathbf{a}_n\right), \\
\mathbf{v}_{n+1} &= \mathbf{v}_n + \Delta t\left((1 - \gamma)\mathbf{a}_n + \gamma\mathbf{a}_{n+1}\right), \\
\mathbf{u}_{n+1} &= \mathbf{u}_n + \Delta t\mathbf{v}_n + \frac{(\Delta t)^2}{2}\left((1 - 2\beta)\mathbf{a}_n + 2\beta\mathbf{a}_{n+1}\right).
\end{aligned}
\tag{27}
$$

These equations directly show that this method is an implicit one. Thus, at each time step a Newton-Raphson iteration is required so as to solve the nonlinear equations (27):

Until convergence is reached, solve the linearized system:

$$
\begin{aligned}
\frac{\partial \mathbf{R}_i^u}{\partial \mathbf{a}_{n+1}}\Delta\mathbf{a} + \frac{\partial \mathbf{R}_i^u}{\partial \mathbf{c}_{n+1}}\Delta\mathbf{c} &= -\mathbf{R}_i^u, \\
\frac{\partial \mathbf{R}_i^c}{\partial \mathbf{a}_{n+1}}\Delta\mathbf{a} + \frac{\partial \mathbf{R}_i^c}{\partial \mathbf{c}_{n+1}}\Delta\mathbf{c} &= -\mathbf{R}_i^c,
\end{aligned}
\tag{28}
$$

with i denoting the current Newton-Raphson iteration and $\mathbf{R}_i^u$ and $\mathbf{R}_i^c$ being the current residuals (see $(27)_{1-2}$). Following Borden et al. [8], convergence can be for instance defined by

$$\max\left\{\frac{||\mathbf{R}_i^u||_{L^2}}{||\mathbf{R}_0^u||_{L^2}}, \frac{||\mathbf{R}_i^c||_{L^2}}{||\mathbf{R}_0^c||_{L^2}}\right\} \leq tol \tag{29}$$

13

with *tol* for example set to 10^{-4}.

Chung and Hulbert [12] have proposed explicit formulas for the parameters. Borden et al. [8] observed that these show a good behaviour in the context of phase-field models of dynamic brittle fracture:

$$
\begin{aligned}
\alpha_f &= \frac{1}{\rho_\infty + 1}, \\
\alpha_m &= \frac{2 - \rho_\infty}{\rho_\infty + 1}, \\
\beta &= \frac{1}{4}\left(1 + \alpha_m - \alpha_f\right)^2, \\
\gamma &= \frac{1}{2} + \alpha_m - \alpha_f,
\end{aligned}
\tag{30}
$$

with spectral radius ρ_∞ of the amplification matrix, describing the numerical dissipation from time step t_n to t_{n+1}. Thus, second-order accuracy and unconditional stability are reached for a second-order linear problem.

4. Conclusion

A phase-field approach for the sake of modelling dynamic fracture has been outlined in this work. A second- and a fourth-order phase-field theory as well as differences between modelling brittle and ductile fracture have been presented. The derivation shown here is based on the variational formulation of brittle fracture which can be seen as a basis for the regularization by the phase-field. Since no variational formulation of ductile fracture has been established yet, the derivation of the governing equations considering ductile fracture is based on microforces and balance laws. Within the phase-field approximation, the length scale parameter l_0 has been introduced. A suitable time integration scheme and shortly, an Isogeometric Analysis framework have been described.

In general, there exist many different setups for modelling fracture with the help of phase-field methods. Since this work is established in a didactic focus, five general differences in these models are mentioned:

1. quasi-static ($\ddot{\mathbf{u}} = \mathbf{0}$) $\leftrightarrow$ dynamic ($\ddot{\mathbf{u}} \neq \mathbf{0}$)
2. 2nd-order- $\leftrightarrow$ 4th-order phase-field theory
3. brittle fracture $\leftrightarrow$ ductile fracture
4. small deformations $\leftrightarrow$ large deformations
5. elasticity $\leftrightarrow$ plasticity (elastoplasticity).

Especially, items 4 and 5 strongly depend on each other. Furthermore, there are several aspects which have not been mentioned in this paper. For example, adaptive mesh refinement should be considered along the crack so as to get a higher resolution of the fracture process. Within the Isogeometric Analysis framework, this can be achieved by using T-Splines or by applying current methods for the local refinement of NURBS (LR NURBS).

So as to conclude this work, advantages of phase-field models of dynamic fracture in contrast to common sharp interface models are presented as well as differences between

14

these approaches are mentioned. Essentially, there are two major differences. At first, the region between damaged and undamaged material is smoothed by the phase-field. As the name already reveals, in sharp interface models there is a discontinuity representing a crack. Secondly, the shown method leads to a new partial differential equation which is coupled to the one enforcing stress equilibrium. In contrast to that, sharp interface models require a great effort on mesh handling and refinement. This aspect already leads to the first great advantage of phase-field methods: The step from 2D to 3D is quite straightforward whereas this step requires much more expense in sharp interface models due to the fact that the mesh handling gets more complicated. Furthermore, the smooth boundary results in the fact that the crack is not a function of the geometry or the mesh, respectively. Often, in sharp interface models the crack is restricted to edges of the mesh which is not the case for the method presented here. Thus, phase-field models do not require numerical tracking of the crack so as to model crack propagation. Actually, this fact makes phase-field methods more uncomplicated. Sharp interface models often suffer in situations with complex crack topologies including branching. This problem can be overcome relative easily by applying the described diffuse interface model. Finally, Borden et al. [7] have shown that the presented fourth-order phase-field theory leads to more accurate results. Since stresses are represented more accurately, the residual stress inside the crack decreases in contrast to the second-order theory. Thus, higher and more realistic crack growth rates can be reached. Additionally, as expected, convergence rates increase for the higher-order model.

All these aspects show the great potential of modelling fracture with the help of phase-fields. This work gives a first insight into this topic and the derivation of the governing equations. Of course, many topics have not been discussed here but in the context of a didactic focus, this paper is thought to introduce and especially, motivate this method and should thus, help with a good start into the subject matter.

Appendix A. Sharp interface models

In this section, shortly, two examples for sharp interface models are illustrated.

Appendix A.1. Virtual crack closure technique

Assuming a two-dimensional plane stress or plane strain model, the *virtual crack closure technique* represents a crack by introducing one-dimensional discontinuities by a line of nodes. The total energy release rate is computed locally at the crack front. If two Finite Elements shall be split by a crack, these elements will not share the same edge and nodes anymore. Thus, new nodes or edges have to be created. So as to handle this problem, there are nodes with identical coordinates at regions where cracks form. If there is no crack yet, these nodes will lie over each other and a multipoint constraint is imposed so as to keep them at the same position. As soon as the respective Finite Elements shall be split, this constraint is disregarded and the two nodes can move apart from each other. Consequently, the elements move apart and a crack within the mesh is introduced. In order to avoid kinematically incompatible self-penetration of elements, an element-wise opening instead of a node-wise opening is required. As shown by Krueger [20], the calculation of the

strain energy release rates, which determine crack nucleation, depend on the element type. Therefore, the formulas used in the computation have to be adapted for different element shapes and varying number of nodes per element. Since these formulas quickly get very complicated, especially for three-dimensional problems, the implementation requires high efforts. Additionally, correction formulas for sharp corners and different element length are required. [20]

Appendix A.2. Cohesive segments method

In the *cohesive segments method*, the crack is represented by a set of overlapping cohesive segments. Thus, the separation process is limited to a set of discrete planes in 3D or discrete lines in 2D, respectively. As soon as a stress state violates a given fracture criterion, a new segment is created. Such a segment adds a discontinuity to an element during calculations by exploiting the partition-of-unity property. For all nodes whose support is cut by a crack into two disjoint pieces or which are crossed by a cohesive segment, respectively, an additional equilibrium equation is given and new degrees of freedom are added. The latter do not affect energy conservation and describe the magnitude of the displacement jump. Within the FE-approximation, this engenders that the approximate displacement field $\mathbf{u}^h = \sum_A N_A \mathbf{u}_A$, where N_A denote the shape functions, is enriched by a discontinuity function and asymptotic crack tip functions which are necessary if a crack does not begin on an edge. However, all this leads to several disadvantages: Quadrature rules have to be adapted, nodes need to have a variable number of degrees of freedom, there is a high accuracy error, the stress state at the tip of a segment is not well described and the specification of the geometry of the cohesive surfaces might lead to problems. [29][30]

Appendix B. Ductile fracture

Already in Section 2.5, the differences between modelling brittle and ductile fracture have been outlined. In the following, energy laws are derived and put together to a thermo-dynamically consistent formulation for ductile fracture.

Ambati et al. [1] proposes a method similar to the one presented for brittle fracture. The major change lies in the Helmholtz free energy (see (13)) which is replaced by

$$\Psi_n = g(c, p) \Psi_e^+(\boldsymbol{\varepsilon}) + \Psi_e^-(\boldsymbol{\varepsilon}) + \Psi_p(\alpha) + \mathcal{G}_c \Gamma_{c,n} \tag{B.1}$$

with the new degradation function $g(c, p) = c^{2p} + \eta$ and $p = \frac{\epsilon_{eq}^p}{\epsilon_{eq,crit}^p}$, $\epsilon_{eq}^p(t) = \sqrt{\frac{2}{3} \int_0^t \sqrt{\dot{\boldsymbol{\varepsilon}} : \dot{\boldsymbol{\varepsilon}}} \mathrm{d}t}$.

The plastic energy density function considering linear isotropic hardening reads $\Psi_p(\alpha) = \sigma_y \alpha + \frac{1}{2} h \alpha^2$ with yield stress σ_y, hardening variable α and hardening modulus $h > 0$. The idea behind this new degradation function is that c depends on p so that the fracture process can be seen as the accumulation of ductile damage. Ψ_p will take the dominating role over Ψ_e^+ and thus, a plasticity-driven fracture initiation is achieved. However, here a more abstract derivation of the governing equations will be presented which is based on the work of Borden et al. [6].

16

In Section 2.1 small deformations and deformation gradients have been assumed. Since this does not hold true for ductile fracture (see Fig. 3), another approach for the derivation of the strong form is chosen. As Borden et al. [6] have outlined, previous approaches on ductile fracture suffer in the fact that yield surface and hardening modulus are not effected by the phase-field's evolution. Thus, at some point plastic strains saturate and deformation is again dominated by recoverable elastic strains. The notation mentioned at the beginning of this section stays the same. The deformation gradient, which cannot be considered small anymore, now reads

$$\mathbf{F} = \frac{\partial \varphi (\mathbf{X}, t)}{\partial \mathbf{X}} \tag{B.2}$$

with deformation map $\varphi : (\Omega_0 \times \mathbb{R}) \rightarrow \mathbb{R}^d$, body Ω_0 in the reference configuration and $\mathbf{x} = \varphi (\mathbf{X}, t)$. (B.2) is now decomposed into the elastic and plastic deformations gradient:

$$\mathbf{F} = \mathbf{F}^e \mathbf{F}^p. \tag{B.3}$$

In contrast to (13), the new stored energy functional proposed by Borden et al. [6] reads

$$\tilde{\Psi} (\mathbf{F}, c, c_{,\mathbf{X}}, \mathbf{F}^p, \alpha) = \int_{\Omega_0} \left[g(c) \Psi^+ (\mathbf{F}, \mathbf{F}^p) + \Psi^- (\mathbf{F}, \mathbf{F}^p) + g_p(c) \Psi_p(\alpha) + \Gamma_{c,n} \right] \mathrm{d}\Omega_0 \tag{B.4}$$

with $(\cdot)_{\mathbf{X}}$ denoting the derivative with respect to $\mathbf{X}$.[3] As in the work by Ambati et al. [1], an effective plastic work contribution Ψ_p depending on the internal hardening variable α has been added. The plastic degradation function $g_p(c)$ provides, analogous to $g(c)$, a mechanism for crack growth driven by the development of plastic strains.

Appendix B.1. Balance laws and strong form

The approach for the derivation of the governing equations is based on balance laws. To keep things short, not every single step of their derivation but more likely their results are presented here. Microforce balance laws are assumed to model the phase-field's evolution within a large deformation setting. The balance of linear momentum and angular momentum in the reference configuration lead to (also see $(14)_1$)

$$Div(\mathbf{P}) + \mathbf{B} = \rho_0 \ddot{\mathbf{U}}, \tag{B.5}$$
$$\boldsymbol{\sigma} = \boldsymbol{\sigma}^T$$

with 1st Piola-Kirchhoff stress tensor $\mathbf{P}$, density ρ_0 in the reference configuration and $Div(\cdot)$ denoting the divergence in the reference configuration. Analogous to this balance law, assuming an internal microforce $\pi(\mathbf{x}, t) \in \mathbb{R}$, an external microforce $l(\mathbf{x}, t) \in \mathbb{R}$ acting on

---

[3]Note that for ductile fracture in this work, $\nabla(\cdot)$ is replaced by the index notation $(\cdot)_{,\mathbf{X}}$ or $(\cdot)_{,\mathbf{x}}$, respectively, in order to distinguish between derivatives with respect to the reference or current configuration. For brittle fracture, everything has been derived within the current configuration.

the body and an external microforce $\lambda\left(\mathbf{x},t\right) = \boldsymbol{\xi} \cdot \mathbf{N}$ acting on the surface (with microforce traction vector $\boldsymbol{\xi}\left(\mathbf{x},t\right) \in \mathbb{R}^d$), the microforce balance leads to

$$Div\left(\boldsymbol{\xi}\right) + \pi + l = 0. \tag{B.6}$$

The energy balance with e_0 describing the internal energy per unit volume reads

$$\frac{\mathrm{d}}{\mathrm{d}t} \int_{\Omega_0} \left(\frac{1}{2}\rho_0|\dot{\mathbf{U}}|^2 + e_0\right) \mathrm{d}\Omega_0 = \int_{\partial\Omega_0} \left(\mathbf{PN}\right) \cdot \dot{\mathbf{U}} \mathrm{d}\partial\Omega_0 + \int_{\Omega_0} \mathbf{B} \cdot \dot{\mathbf{U}} \mathrm{d}\Omega_0 + \int_{\partial\Omega_0} \lambda\dot{c}\, \mathrm{d}\partial\Omega_0 + \int_{\Omega_0} l\dot{c}\, \mathrm{d}\Omega_0, \tag{B.7}$$

where $\dot{c}$ is found to be the work conjugate of the microforces. The second law of thermodynamics leads to

$$\Theta\dot{s} \geq 0 \tag{B.8}$$

with entropy per unit volume s and absolute temperature Θ. Note that heat fluxes and heat sources are not considered here (isothermal and adiabatic process). Using the dissipation inequality $e_0 = \Psi + \Theta s$ (see Legendre transformation), (B.8) can be rewritten as

$$\dot{\Psi} \leq \dot{e}_0 \tag{B.9}$$

with Helmholtz free energy Ψ. Regarding the microforces within the energy balance (B.7), the divergence theorem has to be applied by using that $\lambda\left(\mathbf{x},t\right) = \boldsymbol{\xi} \cdot \mathbf{N}$ and (B.6) has to be plugged in. For the remaining terms, integration by parts leads to

$$\int_{\partial\Omega_0} \left(\mathbf{PN}\right) \cdot \dot{\mathbf{U}} \mathrm{d}\partial\Omega_0 = \int_{\Omega_0} Div\left(\mathbf{P}\right) \cdot \dot{\mathbf{U}} \mathrm{d}\Omega_0 + \int_{\Omega_0} \mathbf{P} : \dot{\mathbf{U}}_{,\mathbf{X}} \mathrm{d}\Omega_0 \tag{B.10}$$

with $\dot{\mathbf{U}}_{,\mathbf{X}} = \dot{\mathbf{F}}$. Inserting $(\text{B.5})_1$ into (B.10) and using that

$$\frac{\mathrm{d}}{\mathrm{d}t}\left(\frac{1}{2}\rho_0|\dot{\mathbf{U}}|^2\right) = \rho_0\dot{\mathbf{U}} \cdot \ddot{\mathbf{U}} \tag{B.11}$$

leads to the following important statement:

A thermodynamically consistent model is achieved as long as Ψ fulfills

$$\int_{\Omega_0} \dot{\Psi} \mathrm{d}\Omega_0 \leq \int_{\Omega_0} \left(\mathbf{P} : \dot{\mathbf{F}} + \boldsymbol{\xi} \cdot \dot{c}_{,\mathbf{X}} - \pi\dot{c}\right) \mathrm{d}\Omega_0 = \int_{\Omega_0} \left(\frac{1}{2}\mathbf{S} : \dot{\mathbf{C}} + \boldsymbol{\xi} \cdot \dot{c}_{,\mathbf{X}}\pi\dot{c}\right) \mathrm{d}\Omega_0. \tag{B.12}$$

$\mathbf{S}$ denotes the 2nd Piola-Kirchhoff stress tensor and $\mathbf{C} = \mathbf{F}^T\mathbf{F}$ the right Cauchy-Green tensor.

Assuming that $\Psi = \Psi\left(\mathbf{C}, \mathbf{C}^p, \mathbf{Q}, c, c_{,\mathbf{X}}, \dot{c}\right)$ with plastic right Cauchy-Green tensor $\mathbf{C}^p = \mathbf{F}^{pT}\mathbf{F}^p$ and set of internal plastic variables $\mathbf{Q}$, applying the chain rule in (B.12) leads to

$$\int_{\Omega_0} \left(\frac{\partial\Psi}{\partial\mathbf{C}} : \dot{\mathbf{C}} + \frac{\partial\Psi}{\partial\mathbf{C}^p} : \dot{\mathbf{C}}^p + \frac{\partial\Psi}{\partial\mathbf{Q}} \cdot \dot{\mathbf{Q}} + \frac{\partial\Psi}{\partial c}\dot{c} + \frac{\partial\Psi}{\partial c_{,\mathbf{X}}} \cdot \dot{c}_{,\mathbf{X}} + \frac{\partial\Psi}{\partial\dot{c}}\ddot{c}\right) \mathrm{d}\Omega_0$$

$$\leq \int_{\Omega_0} \left(\frac{1}{2}\mathbf{S} : \dot{\mathbf{C}} + \boldsymbol{\xi} \cdot \dot{c}_{,\mathbf{X}} - \pi\dot{c}\right) \mathrm{d}\Omega_0. \tag{B.13}$$

18

The plastic dissipation $\mathbb{D}^p = -\dfrac{\partial\Psi}{\partial\mathbf{C}^p} : \dot{\mathbf{C}}^p - \dfrac{\partial\Psi}{\partial\mathbf{Q}} \cdot \dot{\mathbf{Q}}$ can be set to zero for purely elastic deformations. Comparing the terms on the left hand and right hand side of (B.13), the following relations can be derived:

$$
\begin{aligned}
\frac{\partial\Psi}{\partial\dot{c}} &= 0, \\
\frac{\partial\Psi}{\partial c_{,\mathbf{X}}} &= \boldsymbol{\xi}, \\
2\frac{\partial\Psi}{\partial\mathbf{C}} &= \mathbf{S}, \\
\left(\pi + \frac{\partial\Psi}{\partial c}\right)\dot{c} &\leq 0, \\
\mathbb{D}^p &\geq 0.
\end{aligned}
\tag{B.14}
$$

$(B.14)_4$ can be rewritten as

$$
\pi = -\frac{\partial\Psi}{\partial c} - \beta\dot{c} \tag{B.15}
$$

with function $\beta = \beta\left(\mathbf{C}, \mathbf{C}^p, c, c_{,\mathbf{X}}\right) \geq 0$ [4]. Inserting (B.14) and (B.15) into the balance laws $(B.5)_1$ and (B.6) leads to following equations (using $\mathbf{P} = \mathbf{F}\mathbf{S}$):

$$
\begin{aligned}
Div\left(2\mathbf{F}\frac{\partial\Psi}{\partial\mathbf{C}}\right) + \mathbf{B} &= \rho_0\ddot{\mathbf{U}}, \\
Div\left(\frac{\partial\Psi}{\partial c_{,\mathbf{X}}}\right) + l - \frac{\partial\Psi}{\partial c} &= \beta\dot{c}.
\end{aligned}
\tag{B.16}
$$

Considering (B.4), the Helmholtz free energy for ductile fracture reads

$$
\Psi_n\left(\mathbf{C}, \mathbf{C}^p, \mathbf{Q}, c, c_{,\mathbf{X}}\right) = g\left(c\right)\Psi^+\left(\mathbf{C}, \mathbf{C}^p\right) + \Psi^-\left(\mathbf{C}, \mathbf{C}^p\right) + g_p\left(c\right)\Psi_p\left(\mathbf{Q}\right) + \Gamma_{c,n}. \tag{B.17}
$$

Setting $l = 0$ and $\beta = 0$ leads to the governing equations. The stress equilibrium is given by

$$
\begin{cases}
Div\left(2\mathbf{F}\left(g\left(c\right)\dfrac{\partial\Psi^+}{\partial\mathbf{C}} + \dfrac{\partial\Psi^-}{\partial\mathbf{C}}\right)\right) + \mathbf{B} = \rho_0\ddot{\mathbf{U}} & \text{on } \Omega_0 \times (0, T) \\
\mathbf{U} = \mathbf{G} & \text{on } \partial\Omega_{0,\mathbf{G}} \times (0, T) \\
\mathbf{T} = \mathbf{H} & \text{on } \partial\Omega_{0,\mathbf{H}} \times (0, T) \\
\mathbf{U} = \mathbf{U}_0 & \text{on } \Omega_0 \times 0 \\
\dot{\mathbf{U}} = \mathbf{V}_0 & \text{on } \Omega_0 \times 0
\end{cases}
\tag{B.18}
$$

with Piola-Kirchhoff traction vector $\mathbf{T} = \mathbf{P}\mathbf{N}$. Considering the second-order phase-field theory and inserting the two partial derivatives $\frac{\partial\Psi}{\partial c_{,\mathbf{X}}}$ and $\frac{\partial\Psi}{\partial c}$ required in $(B.16)_2$ with the help of (B.17), leads to following equation:

$$
\frac{2l_0}{\mathcal{G}_c^0}\left(g'\left(c\right)\Psi^+ + g_p'\left(c\right)\Psi_p\right) + c - 4l_0^2\Delta c = 1 \quad \text{on } \Omega \times (0, T). \tag{B.19}
$$

---

[4] β can be seen as a dissipation constant.

However, the irreversibility conditions outlined in (15) have not been considered yet. Now, the history field is given by

$$\mathcal{H}\left(\mathbf{C}, \mathbf{C}^p\right) = \max_{\bar{t} \leq t} \Psi^+ \left(\mathbf{C}\left(\bar{t}\right), \mathbf{C}^p\left(\bar{t}\right)\right). \tag{B.20}$$

Having $\langle \cdot \rangle$ defined as in (11), the term Ψ_p in (B.19) is replaced by $\langle \Psi_p - \Psi_0 \rangle$. Actually, Ψ_p is already assumed to be monotonically increasing so that no additional constraints are necessary in order to enforce irreversibility crack growth caused by plastic deformation. However, Borden et al. [6] introduce the plastic work threshold Ψ_0 so as to have more control over the contribution of plastic deformation to crack growth. Thus, if $\Psi_p < \Psi_0$, there will be no contribution of plastic deformation to crack growth. This point can now be controlled easily. Furthermore, Borden et al. [6] introduce parameters $\beta_e \in [0, 1]$ and $\beta_p [0, 1]$ which can be used in order to weight the contributions from elastic strain energy and plastic work to crack growth. These modifications, (B.19) and (B.20) lead to the governing equations for the evolution of the phase-field considering ductile fracture and the second-order phase-field theory:

$$\begin{cases} \dfrac{2l_0}{\mathcal{G}_c^0} \left(\beta_e g'\left(c\right)\mathcal{H} + \beta_p g_p'\left(c\right)\langle \Psi_p - \Psi_0 \rangle\right) + c - 4l_0^2 \Delta c = 1 & \text{on } \Omega_0 \times (0, T) \\[2mm] \hspace{9.5cm} c_{,\mathbf{X}} \cdot \mathbf{N} = 0 & \text{on } \partial\Omega_0 \times (0, T) \\[2mm] \hspace{10cm} c = c_0 & \text{on } \Omega_0 \times 0. \end{cases} \tag{B.21}$$

The boundary conditions on the phase-field result from the homogeneous natural boundary conditions arising from the derivation of the weak form [5].

There are several constitutive models so as to determine the energy density functions Ψ^+, Ψ^- and Ψ_p. These have been well outlined by Borden et al. [6] and within this paper, it is only referred to this work.

Since $(8)_2$ includes second order spatial derivatives of c for the fourth-order phase-field theory, the relations (B.14) have to be adapted. For that, the Helmholtz free energy is assumed to take the form $\Psi = \Psi\left(\mathbf{C}, \mathbf{C}^p, \mathbf{Q}, c, c_{,\mathbf{X}}, c_{,ii}, \dot{c}\right)$ so that (B.13) changes to[5]:

$$\int\limits_{\Omega_0} \left(\frac{\partial \Psi}{\partial \mathbf{C}} : \dot{\mathbf{C}} + \frac{\partial \Psi}{\partial \mathbf{C}^p} : \dot{\mathbf{C}}^p + \frac{\partial \Psi}{\partial \mathbf{Q}} \cdot \dot{\mathbf{Q}} + \frac{\partial \Psi}{\partial c}\dot{c} + \frac{\partial \Psi}{\partial c_{,\mathbf{X}}} \cdot \dot{c}_{,\mathbf{X}} + \frac{\partial \Psi}{\partial c_{,jj}}\dot{c}_{,ii} + \frac{\partial \Psi}{\partial \dot{c}}\ddot{c}\right) \mathrm{d}\Omega_0$$
$$\leq \int\limits_{\Omega_0} \left(\frac{1}{2}\mathbf{S} : \dot{\mathbf{C}} + \boldsymbol{\xi} \cdot \dot{c}_{,\mathbf{X}} - \pi\dot{c}\right) \mathrm{d}\Omega_0. \tag{B.22}$$

So as to compare the terms on the left- and right-hand side and thus, to involve the Laplacian

---

[5]Note that Einstein's summation convention on repeated indices is used here.

of c, the divergence theorem is applied:

$$\int_{\Omega_0} \frac{\partial \Psi}{\partial c_{,jj}} \dot{c}_{,ii} \mathrm{d}\Omega_0 = \int_{\Omega_0} \left[\left(\frac{\partial \Psi}{\partial c_{,jj}} \dot{c}_{,i} \right)_{,i} - \left(\frac{\partial \Psi}{\partial c_{,jj}} \right)_{,i} \dot{c}_{,i} \right] \mathrm{d}\Omega_0$$

$$= \int_{\partial \Omega_0} \frac{\partial \Psi}{\partial c_{,jj}} \dot{c}_{,i} N_i \mathrm{d}\partial \Omega_0 - \int_{\Omega_0} \left(\frac{\partial \Psi}{\partial c_{,jj}} \right)_{,i} \dot{c}_{,i} \mathrm{d}\Omega_0. \tag{B.23}$$

As a consequence, terms can be compared which leads to following new relations:

$$\frac{\partial \Psi}{\partial \dot{c}} = 0,$$
$$\frac{\partial \Psi}{\partial c_{,\mathbf{i}}} - \left(\frac{\partial \Psi}{\partial c_{,jj}} \right)_{,i} = \xi_{,i},$$
$$\frac{\partial \Psi}{\partial c_{,jj}} = 0 \quad \text{on } \partial \Omega_0, \tag{B.24}$$
$$2 \frac{\partial \Psi}{\partial \mathbf{C}} = \mathbf{S},$$
$$\left(\pi + \frac{\partial \Psi}{\partial c} \right) \dot{c} \leq 0,$$
$$\mathbb{D}^p \geq 0.$$

The function β stays the same as in (B.15). Inserting this function and the relations (B.24) into the microforce balance (B.6) leads to the equation

$$\left(\frac{\partial \Psi}{\partial c_{,i}} \right)_{,i} - \left(\frac{\partial \Psi}{\partial c_{,jj}} \right)_{,ii} - \frac{\partial \Psi}{\partial c} - \beta \dot{c} + l = 0. \tag{B.25}$$

Inserting the Helmholtz free energy from (B.17) for $n = 4$ into (B.25) leads to the governing equations for the phase-field's evolution considering the fourth-order phase-field theory:

$$\begin{cases} \frac{2l_0}{\mathcal{G}_c^0} \left(\beta_e g'(c) \mathcal{H} + \beta_p g_p'(c) \langle \Psi_p - \Psi_0 \rangle \right) + c - 2l_0^2 \Delta c + l_0^4 \Delta (\Delta c) = 1 & \text{on } \Omega_0 \times (0, T) \\ \Delta c = 0 & \text{on } \partial \Omega_0 \times (0, T) \\ \nabla \left(l_0^4 \Delta c - 2l_0^2 c \right) \cdot \mathbf{N} = 0 & \text{on } \partial \Omega_0 \times (0, T) \\ c = c_0 & \text{on } \Omega_0 \times 0 \end{cases} \tag{B.26}$$

Note that the threshold Ψ_0 has been added just as for the second-order phase-field theory (see (B.21)). The boundary conditions on the phase-field result from the homogeneous natural boundary conditions arising from the derivation of the weak form [5].

Appendix B.2. Weak and semidiscrete Galerkin form

Analogous to brittle fracture, the weak form for the second-order phase-field theory for ductile fracture can be derived. Considering the critical fracture energy density $\mathcal{G}_c = \frac{\mathcal{G}_c^0}{J}$ in the current configuration with Jacobian J, the system reads:

n=2: Find $\mathbf{u}\left(t\right) \in \boldsymbol{\mathcal{S}}$ and $c\left(t\right) \in \tilde{\mathcal{S}}_2, t \in [0,T]$ so that $\forall \mathbf{w} \in \boldsymbol{\mathcal{V}}$ and $\forall q \in \tilde{\mathcal{V}}_2$:

$$
\begin{cases}
\left(\rho\ddot{\mathbf{u}}, \mathbf{w}\right)_\Omega + \left(\boldsymbol{\sigma}, \nabla\mathbf{w}\right)_\Omega = \left(\mathbf{h}, \mathbf{w}\right)_{\partial\Omega_\mathbf{h}} + \left(\mathbf{b}, \mathbf{w}\right)_{\partial\Omega_\mathbf{g}} \\
\left(\dfrac{2l_0}{J\mathcal{G}_c}\left(\beta_e g'\left(c\right) + \beta_p g'_p\left(c\right)\langle\Psi_p - \Psi_0\rangle\right) + c, q\right)_\Omega \\
\qquad\qquad + \left(4l_0^2 c_{,\mathbf{X}}, q_{,\mathbf{X}}\right)_{\Omega_0} = \left(1, q\right)_\Omega \\
\left(\rho\mathbf{u}\left(0\right), \mathbf{w}\right)_\Omega = \left(\rho\mathbf{u}_0, \mathbf{w}\right)_\Omega \\
\left(\rho\dot{\mathbf{u}}\left(0\right), \mathbf{w}\right)_\Omega = \left(\rho\dot{\mathbf{u}}_0, \mathbf{w}\right)_\Omega \\
\left(c\left(0\right), q\right)_{\Omega_0} = \left(c_0, q\right)_{\Omega_0}.
\end{cases}
\tag{B.27}
$$

The semidiskrete Galerkin form follows as already mentioned for the weak form considering brittle fracture (see Section 3.1). The linearization of $g'\left(c\right)$ is done the same way as in (22). Note that derivatives with respect to the reference configuration can be mapped to derivatives within the current configuration by applying the chain rule $\left(\cdot\right)_{,\mathbf{X}} = \left(\cdot\right)_{,\mathbf{x}}\mathbf{F}$. Thus, the term $\left(4l_0^2 c_{,\mathbf{X}}, q_{,\mathbf{X}}\right)_{\Omega_0}$ in (B.27) becomes $\left(4l_0^2\mathbf{F}^T c^h_{,\mathbf{x}}, \mathbf{F}^T q^h_{,\mathbf{x}}\right)_\Omega$ so that the weak as well as the semidiscrete Galerkin form is stated in the current configuration.

For the fourth-order phase-field theory, the weak form considering ductile fracture reads:

n=4: Find $\mathbf{u}\left(t\right) \in \boldsymbol{\mathcal{S}}$ and $c\left(t\right) \in \tilde{\mathcal{S}}_2, t \in [0,T]$ so that $\forall \mathbf{w} \in \boldsymbol{\mathcal{V}}$ and $\forall q \in \tilde{\mathcal{V}}_2$:

$$
\begin{cases}
\left(\rho\ddot{\mathbf{u}}, \mathbf{w}\right)_\Omega + \left(\boldsymbol{\sigma}, \nabla\mathbf{w}\right)_\Omega = \left(\mathbf{h}, \mathbf{w}\right)_{\partial\Omega_\mathbf{h}} + \left(\mathbf{b}, \mathbf{w}\right)_{\partial\Omega_\mathbf{g}} \\
\left(\dfrac{2l_0}{J\mathcal{G}_c}\left(\beta_e g'\left(c\right) + \beta_p g'_p\left(c\right)\langle\Psi_p - \Psi_0\rangle\right) + c, q\right)_\Omega \\
\qquad + \left(2l_0^2 c_{,\mathbf{X}}, q_{,\mathbf{X}}\right)_{\Omega_0} + \left(l_0^4 \Delta^\mathbf{X} c, \Delta^\mathbf{X} q\right)_{\Omega_0} = \left(1, q\right)_\Omega \\
\left(\rho\mathbf{u}\left(0\right), \mathbf{w}\right)_\Omega = \left(\rho\mathbf{u}_0, \mathbf{w}\right)_\Omega \\
\left(\rho\dot{\mathbf{u}}\left(0\right), \mathbf{w}\right)_\Omega = \left(\rho\dot{\mathbf{u}}_0, \mathbf{w}\right)_\Omega \\
\left(c\left(0\right), q\right)_{\Omega_0} = \left(c_0, q\right)_{\Omega_0}
\end{cases}
\tag{B.28}
$$

where $\Delta^\mathbf{X}$ refers to the Laplacian with respect to the reference configuration. Note that $\Delta^\mathbf{X} c = \sum_i c_{,ii} F_{ii}^2$ with $c_{,ii}$ denoting the second-order derivatives with respect to the current configuration. Thus, the weak form (B.28) and corresponding semidiscrete Galerkin form can be formulated in the current configuration.

The semidiscrete Galerkin forms for both, the second-order and fourth-order model, can be analogously derived as for brittle fracture (see Section 3.1).

Appendix B.3. Residual vectors for the time integration scheme

Analogous to brittle fracture, for the second-order phase-field theory of ductile fracture, the residual vectors based on $(\text{B.27})_2$ within the generalized-α scheme are given by

$$
\begin{aligned}
\mathbf{R}^c &= \{R_A^c\}, \\
R_A^c &= \left(1, N_A\right)_\Omega - \left(\frac{2l_0}{J\mathcal{G}_c}\left(\beta_e g'_{lin}\left(c^h\right) + \beta_p g'_{p,lin}\left(c^h\right)\langle\Psi_p - \Psi_0\rangle\right) + c^h, N_A\right)_\Omega \\
&\quad - \left(4l_0^2 c^h_{,I}, N_{A,I}\right)_\Omega
\end{aligned}
\tag{B.29}
$$

22

and for the corresponding fourth-order theory based on $(B.28)_2$ by

$$
\mathbf{R}^c = \{R_A^c\},
$$

$$
R_A^c = (1, N_A)_\Omega - \left(\frac{2l_0}{J\mathcal{G}_c} \left(\beta_e g'_{lin} \left(c^h \right) + \beta_p g'_{p,lin} \left(c^h \right) \langle \Psi_p - \Psi_0 \rangle \right) + c^h, N_A \right)_\Omega \qquad \text{(B.30)}
$$
$$
- \left(2l_0^2 c_{,I}^h, N_{A,I} \right)_\Omega - \left(l_0^4 c_{,II}^h, N_{A,JJ} \right)_\Omega .
$$

References

[1] Ambati, M., Gerasimov, T., De Lorenzis, L., April 2015. Phase-field modeling of ductile fracture. Computational Mechanics.

[2] Ambrosio, L., Tortorelli, V. M., 1992. On the approximation of free discontinuity problems. Bollettino dell'Unione Matematica Italiana, 105–123.

[3] Amor, H., Marigo, J.-J., Maurini, C., 2009. Regularized formulation of the variational brittle fracture with unilateral contact: Numerical experiments. Journal of the Mechanics and Physics of Solids 57, 1209–1229.

[4] Badnava, H., Etemadi, E., Msekh, M. A., 2017. A phase field model for rate-dependent ductile fracture. Metals.

[5] Borden, M. J., August 2012. Isogeometric analysis of phase-field models for dynamic brittle and ductile fracture. Ph.D. thesis, The University of Texas at Austin.

[6] Borden, M. J., Hughes, T. J. R., Landis, C. M., Anvari, A., Lee, I. J., 2016. A phase-field formulation for fracture in ductile materials: Finite deformation balance law derivation, plastic degradation, and stress triaxiality effects. Computer Methods in Applied Mechanics and Engineering 312, 130–166.

[7] Borden, M. J., Hughes, T. J. R., Landis, C. M., Verhoosel, C. V., 2014. A higher-order phase-field model for brittle fracture: Formulation and analysis within the isogeometric analysis framework. Computer Methods in Applied Mechanics and Engineering 273, 100–118.

[8] Borden, M. J., Verhoosel, C. V., Scott, M. A., Hughes, T. J. R., Landis, C. M., 2012. A phase-field description of dynamic brittle fracture. Computer Methods in Applied Mechanics and Engineering 217-220, 77–95.

[9] Bourdin, B., Chukwudozie, C., Yoshioka, K. (Eds.), 2012. A Variational Approach to the Numerical Simulation of Hydraulic Fracturing. SPE Annual Technical Conference and Exhibition (ATCE).

[10] Bourdin, B., Francfort, G. A., Marigo, J.-J., 2008. The variational approach to fracture. J Elasticity 91, 5–148.

[11] Bourdin, B., Larsen, C. J., Richardson, C. L., 2011. A time-discrete model for dynamic fracture based on crack regularization. International Journal of Fracture 168, 133–143.

[12] Chung, J., Hulbert, G. M., 1993. A time integration algorithm for structural dynamics with improved numerical dissipation: the generalized-alpha method. Journal of Applied Mechanics 60(2), 371–375.

[13] Forsey, D. R., Bartels, R. H. (Eds.), 1988. Hierarchical B-spline refinement. Vol. 22. SIGGRAPH Computer Graphics.

[14] Francfort, G. A., Marigo, J.-J., January 1998. Revisiting brittle fracture as an energy minimization problem. Journal of the Mechanics and Physics of Solids 46 (8), 1349–1342.

[15] Helrich, C. S., 2016. Analytical Mechanics (Undergraduate Lecture Notes in Physics). Springer Verlag.

[16] Hofacker, M., Miehe, C., 2013. A phase field model of dynamic fracture: robust field updates for the analysis of complex crack patterns. International Journal for Numerical Methods in Engineering 93, 276–301.

[17] Hughes, T. J. R., Cottrell, J. A., Bazilevs, Y., 2015. Isogeometric analysis: Cad, finite elements, nurbs,exact geometry and mesh refinement. Computer Methods in Applied Mechanics and Engineering 194, 4135–4195.

[18] Irzal, F., Remmers, J. J. C., Verhoosel, C. V., de Borst, R., 2013. An isogemetric analysis bézier interface

element for mechanical and poromechanical fracture problems. International Journal for Numerical Methods in Engineering 97, 608–628.

[19] Karma, A., Kessler, D. A., Levine, H., 2001. Phase-field model of mode iii dynamic fracture. Physical Review Letters 87.

[20] Krueger, R., March 2004. Virtual crack closure technique: History, approach and applications. Applied Mechanics Reviews 57 (2).

[21] Larsen, C. J. (Ed.), 2010. Models for dynamic fracture based on Griffiths criterion. Vol. 21. IUTAM Symposium on Variational Concepts with Applications to the Mechanics of Materials.

[22] Larsen, C. J., Ortner, C., Süli, E., 2010. Existence of solutions to a regularized model of dynamic fracture. Mathematical Models and Methods in Applied Sciences 20 (7), 1021–1048.

[23] Miehe, C., Hofacker, M., Welschinger, F., 2010. A phase field model for rate-independent crack propagation: Robust algorithmic implementation based on operator splits. Computer Methods in Applied Mechanics and Engineering 199, 2765–2778.

[24] Miehe, C., Schänzel, L.-M., 2014. Phase field modeling of fracture in rubbery polymers. part i: Finite elasticity coupled with brittle failure. Journal of the Mechanics and Physics of Solids 65, 93–113.

[25] Miehe, C., Schänzel, L.-M., Ulmer, H., 2015. Phase field modeling of fracture in multi-physics problems. part i. balance of crack surface and failure criteria for brittle crack propagation in thermo-elastic solids. Computer Methods in Applied Mechanics and Engineering 294, 449–485.

[26] Miehe, C., Welschinger, F., Hofacker, M., 2010. Thermodynamically consistent phase-field models of fracture: Variational principles and multi-field fe implementations. International Journal for Numerical Methods in Engineering 89, 1273–1311.

[27] Mikelić, A., Wheeler, M. F., Wick, T., 2015. A phase-field method for propagating fluid-filled fractures coupled to a surrounding porous medium. SIAM Multiscale Modeling and Simulation 13, 367–398.

[28] Quoc Bui, T., Hirose, S., Zhang, C., Rabczuk, T., Wu, C.-T., Saitoh, T., Lei, J., 2016. Extended isogeometric analysis for dynamic fracture in multiphase piezoelectric/piezomagnetic composites. Mechanics of Materials 97, 135–163.

[29] Remmers, J. J. C., de Borst, R., Needleman, A., 2003. A cohesive segments method for the simulation of crack growth. Compuational Mechanics 31, 69–77.

[30] Remmers, J. J. C., de Borst, R., Needleman, A., 2008. The simulation of dynamic crack propagation using the cohesive segments method. Journal of the Mechanics and Physics of Solids 56, 70–92.

[31] Sederberg, T. W., Zheng, J., Bakenov, A., Nasri, A. (Eds.), 2003. T-Splines and T-NURCCS. Vol. 22. Transactions on Graphics (TOG).

[32] Wilson, Z. A., Borden, M. J.and Landis, C. M., 2013. A phase-field model for fracture in piezoelectric ceramics. International Journal of Fracture 183, 135–153.

[33] Zimmermann, C., Sauer, R. A., 2017. Adaptive local surface refinement based on LR NURBS and its application to contact. Computational Mechanics.